Upper-Oceanic Warming in the Gulf of Mexico between 1950 and 2020

ZHANKUN WANG,[a,b] TIM BOYER,[c] JAMES REAGAN,[c] AND PATRICK HOGAN[b]

[a] *NOAA/National Centers for Environmental Information, Stennis Space Center, Mississippi*
[b] *Northern Gulf Institute, Mississippi State University, Stennis Space Center, Mississippi*
[c] *NOAA/National Centers for Environmental Information, Silver Spring, Maryland*

(Manuscript received 29 May 2022, in final form 20 December 2022)

ABSTRACT: We estimate ocean heat content (OHC) change in the upper 2000 m in the Gulf of Mexico (GOM) from 1950 to 2020 to improve understanding of regional warming. Our estimates are based on 192 890 temperature profiles from the World Ocean Database. Warming occurs at all depths and in most regions except for a small region at northeastern GOM between 200 and 600 m. GOM OHC in the upper 2000 m increases at a rate of 0.38 ± 0.13 ZJ decade^{-1} between 1970 and 2020, which is equivalent to 1.21 ± 0.41 terawatts (TW). The GOM sea surface temperature (SST) increased ~1.0° ± 0.25°C between 1970 and 2020, equivalent to a warming rate of 0.19° ± 0.05°C decade^{-1}. Although SST in the GOM increases at a rate approximately twice that for the global ocean, the full-depth ocean heat storage rate in the GOM (0.86 ± 0.26 W m^{-2}) applied to the entire GOM surface is comparable to that for the global ocean (0.82–1.11 W m^{-2}). The upper-1000-m layer accounts for approximately 80%–90% of the total warming and variations in the upper 2000 m in the GOM. The Loop Current advective net heat flux is estimated to be 40.7 ± 6.3 TW through the GOM. A heat budget analysis shows the difference between the advective heat flux and the ocean heat storage rate (1.76 ± 1.36 TW, 1992–2017) can be roughly balanced with the annual net surface heat flux from ECCO (−37.9 TW).

KEYWORDS: Advection; Climate change; Energy budget/balance; Heat budgets/fluxes; Temperature

1. Introduction

The ocean heat content (OHC) of the global ocean has increased significantly over the past few decades (Levitus et al. 2012; IPCC 2021). Although oceanic warming is a global phenomenon, its manifestations and consequences are different regionally. Therefore, quantifying warming/cooling trends on a regional scale is critical to understanding the impacts and conducting risk assessments for ecologically and economically significant marginal seas, such as the Gulf of Mexico (GOM). Most oceanic warming research has been focused on a global scale, with some exceptions (e.g., equatorial Indian Ocean; Alory and Meyers 2009; Gulf of Maine; Seidov et al. 2021). Very little research is available regarding detailed spatiotemporal distributions of the warming/cooling in the upper water of the GOM (Ochoa et al. 2021; Li et al. 2022). Temperature profiles have been collected in the GOM since the 1920s and are freely available via the World Ocean Database. In this manuscript, we use the temperature profiles from the World Ocean Database 2018 (WOD18; Boyer et al. 2018) and its updates collected between 1950 and 2020 to quantify the OHC trend in the GOM.

Previous studies on oceanic warming in the GOM are mostly restricted to sea surface temperature (SST) changes (e.g., Glenn et al. 2015; Muller-Karger et al. 2015; Li et al. 2022) and deep-water warming (Ochoa et al. 2021). Glenn et al. (2015) studied the SST warming trend for the Caribbean and surrounding regions (including GOM) between 1982 and 2012 using an optimum-interpolated SST product. They found a regional increase in annual average SST of 0.15°C decade^{-1} for the period 1982–2012 in the Caribbean and Gulf of Mexico, which was larger than the annual global rate of 0.11°C decade^{-1} during the same period. They also indicated that the warming was likely influenced by El Niño–Southern Oscillation (ENSO) based on cross-correlation analysis. Muller-Karger et al. (2015) found that SST, wind speed, and sea surface height anomaly (SSHA) showed a statistically significant increase between the early 1980s and 2012 in the GOM. The increase in SST anomaly ranged between 0.17° and 0.3°C decade^{-1} in the interior (depth > 1000 m) GOM. Li et al. (2022) characterized the spatial patterns of the monthly trends in SST of the GOM and investigated the seasonal variations in warming trends using satellite SST between 1982 and 2019. They found that the summer warming trend (0.22°C decade^{-1}) was larger than the winter trend (0.05°C decade^{-1}), suggesting seasonal variations of surface warming in the GOM. Regional datasets for the Florida Keys outer reef showed 0.8°–0.9°C of warming in sea surface temperature over the twentieth century and can be fully accounted for by the warming observed from 1975 to 2007 (Kuffner et al. 2015). In a study of Hurricane Harvey, Trenberth et al. (2018) discovered that OHC for the upper 160 m was the highest on record in the GOM prior to the beginning of the summer of 2017, which not only increased the fuel availability for Hurricane Harvey intensification, but also increased flooding rains on land. Ochoa et al. (2021) studied deep-water warming in the western GOM between 2003 and 2019. They found a stable linear warming trend of 0.016° ± 0.002°C decade^{-1} at about 3500 m using near-bottom

Denotes content that is immediately available upon publication as open access.

Corresponding author: Zhankun Wang, zhankun.wang@noaa.gov

DOI: 10.1175/JCLI-D-22-0409.1

measurements at four sites between 2007 and 2018 and a rate of approximately 0.018° ± 0.002°C decade^{-1} below 2000 m between 2003 and 2019 using CTD data from eight oceanographic cruises. The change of the OHC and the warming/cooling trend in the upper 2000 m of the GOM are still unclear. The present study will fill in the gap about the OHC change in the upper 2000 m using WOD temperature profiles, which allow us to extend satellite-only analyses backward in time and also allow us to diagnose trends at deeper depths.

Knowing how the warming/cooling trend varies on different spatial and temporal scales is critical for understanding the consequences of oceanic climate change and climate variability in the GOM. The increased temperature can affect many aspects of the natural environment and ecosystem in the GOM, including coral reefs (Jordán-Dahlgren et al. 2005; Lunden et al. 2014), Atlantic bluefin tuna (Muhling et al. 2011), and poleward organisms distribution shift (Fodrie et al. 2010). The GOM is a semienclosed marginal sea that extends from 17.5° to 31.5°N and from 98° to 80°W. It has a long coastline with ~4.9% of the U.S. population living along the GOM coast (Cohen 2018; McKinney et al. 2021). It forms a complex semienclosed system with interactions among physical, biogeochemical, socioeconomic, and human activities. GOM ecosystems are vulnerable to climate change impacts and threatened by habitat degradation, ecosystem fragmentation, and increased population growth along the coast (McKinney et al. 2021).

Estimating and analyzing the OHC is essential for understanding the evolution of the GOM long-term warming/cooling trend. Following Levitus et al. (2012), we use the term "ocean heat content" instead of "ocean heat content anomaly" used in some publications because OHC is always computed with a reference mean subtracted from each observation. In this paper, using OHC estimated from the objectively analyzed pentadal anomaly temperature fields (observations interpolated to standard levels subtracted from the *World Ocean Atlas 2009* climatological mean temperature field; Locarnini et al. 2018) from the WOD (Boyer et al. 2018), we investigate the spatial and temporal distribution of the OHC change over the past 70 years and quantify the warming trend in the GOM. We further discuss the heat budget closure in the GOM using the net surface heat flux from multiple heat flux products and the estimated Loop Current net advective heat flux.

2. Data and methods

a. Data

The warming trend in the GOM is quantified using running pentadal (5-yr) objectively analyzed gridded temperature anomaly fields. The temperature data used to generate the pentadal gridded fields include 192 890 temperature profiles (Fig. 1) collected between 1948 and 2020 in the WOD18 (Boyer et al. 2018) and its updates. WOD is the world's largest collection of publicly available ocean profile data. The instrument and platform (vehicle from which the instruments were deployed), years of use, and standard deepest depths of measurement are shown in Table 1.

Reversing thermometers attached to bottles and later conductivity–temperature–depth (CTD) sensors have been deployed in most years from research ships by U.S. universities, mainly those in proximity to the Gulf, notably Texas A&M, the University of Southern Mississippi, Louisiana State University, and the University of Miami. NOAA research ships provide a major contribution of bottle/CTD temperature profiles from research and monitoring programs. There are also contributions from Mexican and Cuban research ships historically. Though not many in overall numbers, bottle and CTD measurements are often full depth (surface to ocean bottom), calibrated, and of high quality and cover the entire Gulf.

From 1948 to 1968, mechanical bathythermographs (MBT) were the main observing system for subsurface temperature both globally and in the GOM. The MBT data, which could be obtained from a moving ship, were used in weather and climate forecasting and covered the entire Gulf, but only to depths of 125 m and later ~250 m. MBT temperature profiles were made mainly from research and U.S. Navy ships. The expendable bathythermograph (XBT) improved on the MBT in that it could be deployed from a moving ship at normal cruise speed. Ships of opportunity now included merchant ships and the XBT quickly became the main ocean subsurface observing system in the Gulf. Air drop XBTs (AXBT) were also used in Gulf-wide observational experiments in the 1970s, but in more recent years have been limited to hurricane drops. XBTs reached depths of 460 m initially, later 760 m, with some AXBTs and ship based XBTs reaching 1830 m depth.

With the advent of the Argo autonomous profiling float program in 2000 (Wong et al. 2020), XBT deployment was cut back significantly globally and in the Gulf. Some pre-Argo profiling floats were deployed in the Gulf but the Argo program initially focused on the open ocean. Starting in 2010, Argo floats were deployed in the Gulf of Mexico. Argo floats record temperature profiles every 5 or 10 days from 2000 m to the surface. In between, floats drift at 1000 m depth. The coverage of Argo floats is the entire Gulf, excepting the shelf and coastal regions. In addition to Argo floats from the U.S. and Mexican Argo programs, there is a small contribution of Air-Launched Autonomous Micro Observer (ALAMO) profiling floats. Gliders, autonomous remotely controlled ocean vehicles which can make high time and space frequency measurements (Lee and Rudnick 2018) have been increasingly used in the Gulf since 2010. Gliders flown by Texas A&M and other Gulf proximate U.S. universities, as well as by the U.S. Navy, have provided coverage of the northern half of the Gulf. Many gliders are deployed to explore the mixed layer, but some dive to 1000 m depth.

Overall, the temperature profiles provide over 80% coverage of the entire GOM at the sea surface in most pentadal periods, except for the period between 2006 and 2010 (Figs. 1 and 2). The data density is higher in the northern GOM than the southern GOM in almost all years. The eastern Gulf usually has a larger data density than the western Gulf. All

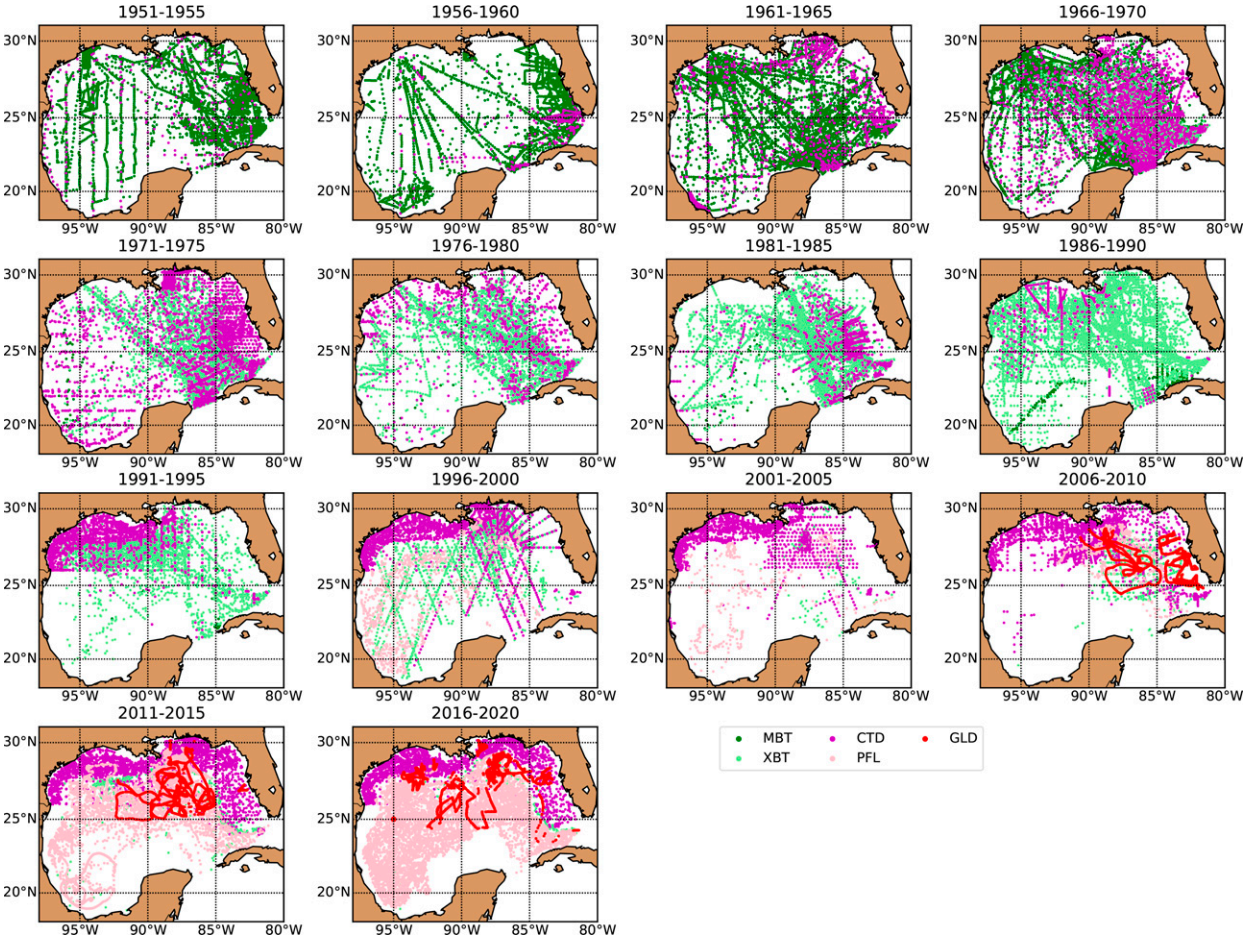

FIG. 1. Temperature profiles' spatial distribution for every pentadal (5-yr) period from 1951 to 2020. The color shows different measurement types. MBT: mechanical bathythermograph data, digital BT (DBT), and microBT (μBT); XBT: expendable bathythermograph and AXBT; CTD: bottle, conductivity–temperature–depth (CTD), expendable CTD (XCTD) data; GLD: glider data; PFL: profiling float data, mainly from the Argo program. Some of the data points may not be shown due to data overlap.

WOD18 temperature profiles are analyzed in a consistent manner by a series of quality control (QC) procedures. The QC includes duplicate elimination, range and gradient checks, statistical checks, and subjective flagging, etc. More details on data sources, data quality control, and data processing procedures as well as objective analysis methods can be found in Boyer et al. (2018) and Locarnini et al. (2018).

b. *Pentadal objective analysis*

To calculate the OHC, the data need to be gridded and gaps need to be filled. We use running pentadal (5-yr) objective analysis to create 1° × °1° gridded temperature anomaly fields at standard depth levels for running pentad from 1950 to 2020. More about pentadal objective analysis can be found in Levitus et al. (2012). The pentad is used in our analysis to ensure sufficient data distribution. Figure 2 shows the temperature data coverage in percentage as a function of time (years) and depth (m) for the pentadal running analysis. The percentage coverage is computed based on the 1° × 1° gridded number of observations. For any grid at any standard depth, at least one observation is needed to be considered having data. Only data with WOD flag = 0 are used. The data coverage is greater than 70% in the upper 100 m in all the years between 1950 and 2020 except in the late 2000s. In the upper 750 m, the data have relatively good coverage with a percentage greater than 70% in most years after 1965, primarily due to the usage of XBT, which measures temperature down to the depth of about 760 m from moving ships. Below 760 m the coverage is lower except after 2010 when CTD and Argo became the dominant instruments. The hatched areas in Fig. 2 show the percent coverage of less than 30% to mask the low coverage periods.

To obtain temperature anomalies for each 1° grid at every standard depth level, we subtract the 1° mean temperature from a monthly climatological value. We use the monthly climatological temperature fields from the *World Ocean Atlas 2009* (*WOA09*) as the reference fields. XBT/MBT biases are corrected following Levitus et al. (2009). The same objective analysis procedure as in Locarnini et al. (2018) and

TABLE 1. Temperature profiles in the Gulf of Mexico by instrument/platform type.

Years	Instrument/platform	No. of profiles	Depth range
1950–2020	Bottle (reversing thermometer) and conductivity–temperature–depth (CTD) from research ship	43 353	Full depth
1967–2020	Expendable bathythermograph (XBT) from ship of opportunity	36 662	460, 760, 1830 m
1948–1994	Mechanical bathythermograph (MBT) from ship of opportunity	27 909	125, 250 m
2010–2019	CTD from glider	71 948	1000 m
1999–2020	CTD from profiling float (mainly Argo)	13 017	2000 m

Levitus et al. (2012) is applied to these temperature anomaly values to create a gridded objectively analyzed temperature anomaly field for each standard depth level for each year (with 80% overlap). A first-guess field of zero is used for the temperature anomaly objective computations, which is a conservative estimate by assuming no change from climatological mean. This will underestimate the warming trend in areas and periods with low data coverage (data density). Given the good data coverage shown in Fig. 2, we expect that it is not a large underestimate in the GOM because the first-guess field (zero) remains only there are no data at all within an ~800 km radius (the influence radius of the objective analysis; Levitus et al. 2012). Caution should be taken when examining the results in poor-data-coverage regions and periods.

c. Ocean heat content

OHC is based on 1° gridded, interpolated temperature anomaly fields T'_w at standard depth levels. The OHC at gridbox $[i, j]$ can be estimated as

$$\mathrm{OHC}(\mathbf{x};t) = \rho_w c_{pw} \int_{\mathrm{D1}}^{\mathrm{D2}} T'_w(\mathbf{x}, z;t)dz, \tag{1}$$

where $\mathbf{x}$ is a horizontal coordinate vector ($\mathbf{x} = [i, j]$), $\rho_w = 1026\ \mathrm{kg\ m^{-3}}$ is the seawater density, $c_{pw} = 3995\ \mathrm{J\ kg^{-1}\ °C^{-1}}$ is the specific heat capacity of seawater, D1 is the upper depth, D2 is the lower depth, z represents depth, and t is time.

Integrated OHC can be estimated by integrating OHC at each grid box over area and depth range in a selected region. The warming/cooling rate can then be determined by ocean heat storage rate Q_t, which is defined as the time derivative of OHC (Etter 1983):

$$Q_t = \frac{\partial \mathrm{OHC}}{\partial t}. \tag{2}$$

The OHC analysis for this study was conducted on both basin and grid levels. The linear statistical trend was calculated as OHC change with time using simple linear regression if the p value was less than 0.05. Linear regression and standard error estimate are conducted using the Python SciPy.stats module. The 95% confidence interval is used in the uncertainty estimate. Autocorrelation was tested in the OHC residuals from the regression analysis using Durbin–Watson statistic. If autocorrelation needed to be considered, the effective degrees of freedom (effective sampling size) were determined based on the e-folding decay time of autocorrelation (Panofsky and Brier 1958) and later used to evaluate standard errors and 95% confidence intervals for uncertainty estimates.

d. Ocean heat budget

The Gulf of Mexico is semienclosed basin and this provides a convenient opportunity to study the heat budget. The heat budget of an oceanic water column may be calculated as follows (Etter 1983):

$$Q_t = Q_{\mathrm{net}} + Q_v, \tag{3}$$

where Q_{net} is the net ocean surface heat flux and Q_v denotes the divergence of the heat transport by ocean currents (advective heat flux). The bottom geothermal heat flux is small in the GOM (Ochoa et al. 2021) and can be ignored in our analysis.

The net ocean surface heat flux Q_{net} comprises net shortwave radiation flux (Q_{SWR}), net longwave radiation flux (Q_{LWR}), surface latent heat flux (Q_{LAT}), and surface sensible heat flux (Q_{Sen}):

$$Q_{\mathrm{net}} = Q_{\mathrm{SWR}} + Q_{\mathrm{LWR}} + Q_{\mathrm{LAT}} + Q_{\mathrm{Sen}}; \tag{4}$$

Q_{net} reflects the complex interaction between the ocean and the atmosphere (Carton et al. 2018). Knowing the annual net surface heat flux is important for understanding the heat budget in the GOM. In this study, we analyze the Q_{net} from four

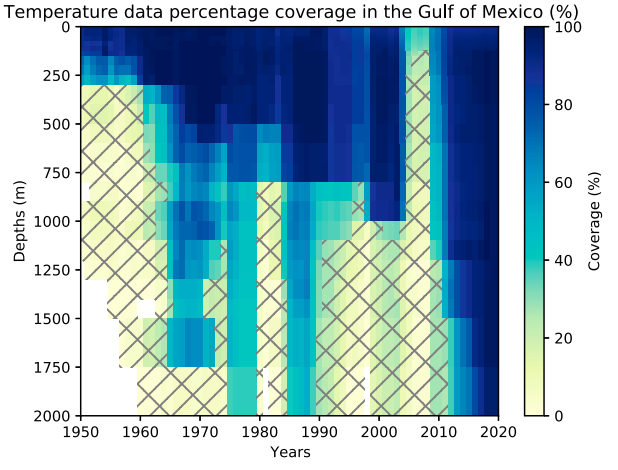

FIG. 2. Percentage of data coverage of 1° squares with at least one observational profile. Hatched area indicates the percentage of coverage less than 30%.

representative products: a fifth-generation atmospheric reanalysis of the global climate covering the period from January 1979 to the present (ERA5; Hersbach et al. 2020) from the European Centre for Medium-Range Weather Forecasts, the objectively analyzed air–sea fluxes (OAFlux; Yu et al. 2008), NASA's Estimating the Circulation and Climate of the Ocean (ECCO version 4; Forget et al. 2015) product, and the Simple Ocean Data Assimilation (SODA; Carton et al. 2018) improved reanalysis data.

Advective heat flux Q_v can be given by

$$Q_v = \rho_w c_{pw} V \delta T, \tag{5}$$

where V is the Loop Current transport, which may be determined by the volume transport across the Yucatán Channel (or Straits of Florida). δT is the average climatology temperature difference between the Yucatán Channel and Straits of Florida. Bunge et al. (2002) and Candela et al. (2019) showed that the volume transport across the Yucatán Channel V_Y and the Florida Straits V_F should be balanced out ($V_Y \approx V_F \approx V$) on a multiple-year time scale because river runoff and the volume transport due to precipitation minus evaporation are very small in the GOM (~0.1% of V; Etter 1983; Bunge et al. 2002) and the change of total volume of water in the GOM with time is also a small term based on altimetry measurements (Bunge et al. 2002).

3. Results

a. Warming trend at sea surface

Figure 3 shows the average surface temperature anomaly as a function of time for the GOM (red lines), the global ocean (black lines), and the subtropical northern Atlantic Ocean within the latitudinal band between 17.5° and 31.5°N (blue lines). The region we selected in the Atlantic Ocean has the same latitudinal band as in the GOM for comparison purposes. There is a persistent warming trend in the Gulf of Mexico with a warming rate of ~0.193°C decade^{-1} starting from around 1970 and the average temperature has increased by ≥1.0°C since 1970. The rate of warming in the Gulf of Mexico is about twice that for the global ocean (0.086°C decade^{-1}), but only slightly larger than the warming trend in the subtropical northern Atlantic Ocean (0.183°C decade^{-1}). This indicates that the subtropical northern Atlantic Ocean, including the GOM, likely has a larger warming rate than that for the global ocean and also shows the linkage between GOM and the tropical northern Atlantic Ocean. We also compared the GOM temperature anomaly at 0 m with that at 10 m and they are very similar (Fig. 3).

Our estimated warming rate of 0.193° ± 0.05°C decade^{-1} for the surface water of GOM is within the range of the rates (0.17°–0.3°C decade^{-1}) estimated by Muller-Karger et al. (2015) in the GOM based on satellite observed SST. Both our estimate and those by Muller-Karger et al. (2015) are slightly larger than the warming rate (0.15°C decade^{-1}) for the Caribbean Sea estimated by Glenn et al. (2015) and the value (0.158°C decade^{-1}) in Li et al. (2022). Levitus et al. (2012) showed the warming rates varied along latitudes for both

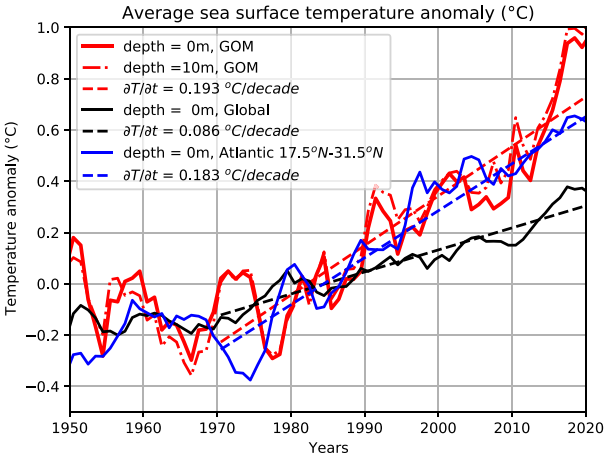

FIG. 3. Time series of the sea surface average temperature anomaly for the Gulf of Mexico (red), northern subtropical Atlantic Ocean between 17.5° and 31.5°N latitudes (blue), and global oceans (black) based on running pentadal (5-yr) analyses. The anomalies are related to a 1955–2006 (*WOA09*) baseline. Each pentadal estimate is plotted at the midpoint of the 5-yr period. The dashed lines show the linear regression fitted lines for the period between 1970 and 2020 for the GOM, global, and the subtropical northern Atlantic Ocean, respectively.

global and basin-scale oceans. Within the same latitudinal band, the warming rate of the GOM and the northern Atlantic Ocean are similar (Fig. 3). Nonetheless, the surface warming rate in the GOM and surrounding oceans based on our estimates and estimates from previous studies are much larger (twice) than the warming rate of the global ocean (0.086°C decade^{-1}). The faster warming rate at the sea surface may make the ecosystem and environment of GOM an area of higher susceptibility to climate change.

b. Subsurface warming

Figure 4a shows the temporal evolution and vertical distribution of the integrated OHC at each standard depth level for the GOM from 0 to 2000 m. The y axis is depth and the x axis is time in years. The OHC is scaled by the thickness of each layer to make it comparable between layers as the thickness of the standard depths varies with depth. The same hatched areas as in Fig. 2 are plotted to show the poor data coverage periods. The vertical profile of the warming rates at each standard depth is shown in Fig. 4b. Simple linear regression is applied to compute the warming rate at each standard depth level and the gray area shows the variation of the warming rates with depth in Fig. 4b. The warming trend is most prominent near the surface in the upper 50 m (Figs. 4a,b). The subsurface OHC change is more complicated. The warming rate rapidly declines with depth from 1.1×10^{17} to 2.5×10^{16} J m^{-1} yr^{-1} from 50 to 400 m. The decline of warming rates decreases below 400 m and becomes more uniform below 1100 m. Between 200 and 600 m, a subsurface irregular decadal warming and cooling oscillation (Fig. 4a) is found, which can also be seen from the integrated 200–600 m OHC shown in Fig. 4c. The entire vertical profile in Fig. 4b (black

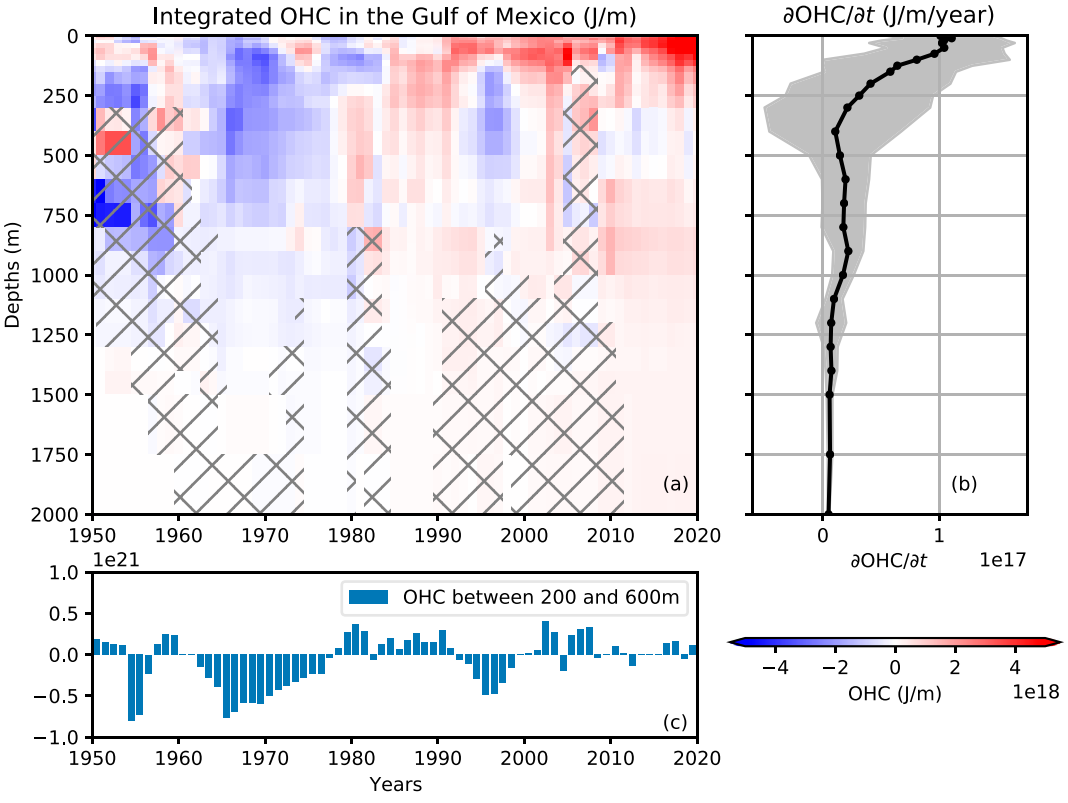

FIG. 4. (a) Spatially integrated OHC in the Gulf of Mexico between 1950 and 2020 as a function of depth (0–2000 m) at standard depths. Hatched indicates the data coverage that is less than 30%. (b) The linear trend of OHC change in the GOM at standard depth levels. The rate is divided by the thickness of each layer to make them vertically comparable. The shading area shows the uncertainty of the linear trends (95% confidence intervals). The trend is estimated using linear regression for each standard depth between 1970 and 2020. The trends are statistically significant at all depths (p value ≤ 0.05). Standard depths are defined as 0, 10, 20, 30, 50, 75, 100, 125, 150, 200, 250, 300, 400, 500, 600, 700, 800, 900, 1000, 1100, 1200, 1300, 1400, 1500, 1750, and 2000 m. Anomalies are relative to a 1955–2006 baseline. (c) Vertically integrated OHC between 200 and 600 m.

line) is positive indicating that oceanic warming occurs at all depths between surface and 2000 m in the GOM. Ochoa et al. (2021) found that the deep water below 2000 m to the seafloor in the GOM was also warming in recent years. According to the warming trends in the upper 2000 m shown in Fig. 4 and the warming shown in Ochoa et al. (2021) below 2000 m, we can conclude that the overall trend of the entire GOM is warming in the past several decades from surface to bottom. Moreover, the Gulf of Mexico has warmed continuously since 1970 (Figs. 3 and 4) and the trend becomes steeper after 2010, at least at the surface (Fig. 3). The data coverage below 750 m reduces substantially. There is much less spatial variability in the GOM temperature field below 750 m than that is above. The seasonal cycle is also very small where it exists below 750 m and by 1000 m, the entire GOM basin is approaching uniformity in temperature. A fewer number of spatially distributed measurements can represent the temperature anomaly of the basin below 750 m.

The causes of the irregular subsurface decadal oscillation between 200 and 600 m need more investigation. The period is approximately 10–30 years, much shorter than the Atlantic multidecadal oscillation (AMO), which has an estimated period of 60–80 years (McCarthy et al. 2015). Sediment core–derived annual SST indicated that AMO-like oscillations could occur in the Gulf of Mexico (Poore and Brock 2011), but our dataset is only 70 years long and we do not have enough evidence to link the decadal oscillation to AMO. The period is closer to that of the North Atlantic Oscillation (NAO), but NAO is largely an atmospheric phenomenon (Hurrell 1995). Our surface OHC does not show clear decadal oscillations as in the subsurface, and thus, the subsurface oscillation is unlikely related to NAO. The interannual and decadal variability of the Loop Current transport flow through the Yucatán Channel may be one possible mechanism to explain the subsurface OHC oscillations between 200 and 600 m, which needs long-term observations (at least decades) of both current and temperature data at the Yucatán Channel to examine this, which currently is not available. Transport flow through the Yucatán Channel has only been measured in recent years but has already shown some interannual

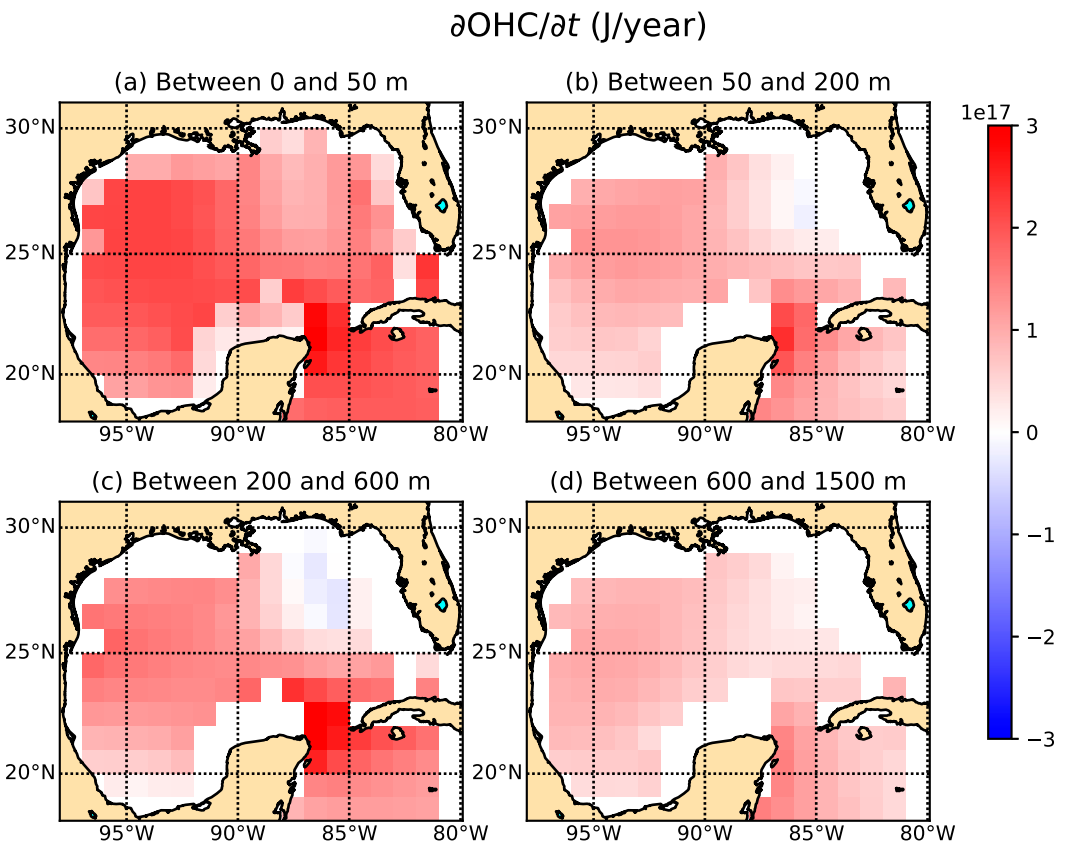

FIG. 5. Spatial distribution of the OHC change with time (units: J yr^{-1}) between different layers (a) 0–50, (b) 50–200, (c) 200–600, and (d) 600–1500 m. The OHC trends are estimated using linear regression between 1970 and 2020 at each grid point between different depth layers.

variations (Candela et al. 2019). More will be discussed in section 4a.

c. *Spatial variations of the warming trends*

To have a more detailed description of the spatial variations of the warming trends, we calculate the heat storage rate for each grid box between selected depth ranges using linear regression between 1970 and 2020. In Fig. 5, we plot the color-coded heat storage rate at each grid box for different selected depth layers. Besides the grids inside the GOM, we also show part of the Yucatán Basin of the Caribbean Sea in Fig. 5. Those grids in Yucatán Basin are not used in the trend estimates for the GOM in Figs. 3 and 4. Similar to what was shown in Fig. 4, the general trend in the upper 50 m (Fig. 5a) is warming, although the warming rate in the northeast Gulf is lower. The warming is largest in the midwestern GOM and at the Yucatán Channel in the upper 50 m. Between 50 and 600 m (Figs. 5b,c), there is a slight cooling trend in the northeast GOM. The rest of the GOM is warming with the Yucatán Channel having the largest warming rate over the entire GOM between 50 and 600 m. Below 600 m, warming occurs almost everywhere and the warming rate is smaller and more uniform. In summary, most of the Gulf of Mexico are warming in recent 50 years in the upper 2000 m except for a small region in the northeastern GOM between 50 and 600 m.

4. Discussion

a. *Ocean heat budget closure*

Based on Eq. (3), the rate of heat storage can be balanced with the annual net surface heat flux and the annual net advective heat flux, which are the two main forcings controlling the OHC change in the GOM. The GOM is a semienclosed basin with two narrow channels—Yucatán Channel and Straits of Florida—connecting with the surrounding oceans. The geographical structure of the GOM makes it an ideal marginal sea to study the ocean heat budget closure. We will quantify all three terms in Eq. (3) to examine the heat budget balance in the GOM.

1) Estimate of heat storage rate Q_T

In Fig. 6, we plot the color-coded OHC between selected layers for the entire GOM in the upper 2000 m. The OHC becomes positive around 1980. About half of the warming after 1980 has occurred in the upper 200 m and the upper 1000 m accounts for 80%–90% of the warming in the upper 2000 m. The heat storage rate of the upper 2000 m in the GOM can be estimated from the integrated OHC using linear regression. Although there are periods of cooling (e.g., 1962–71, 1992–2000) in the GOM, a warming trend is clear between 1970 and 2020 based on the integrated OHC in the upper 2000 m (Fig. 6).

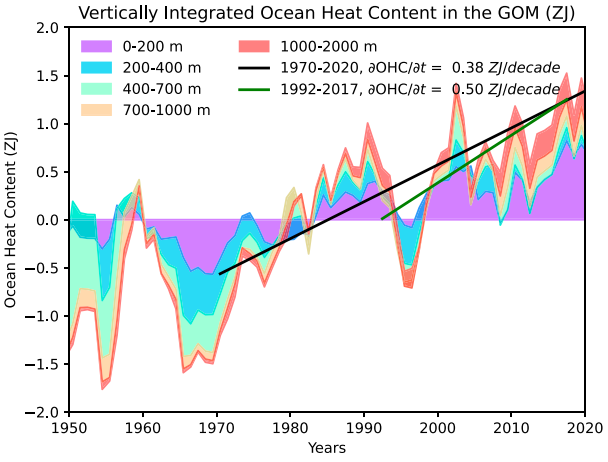

FIG. 6. Vertically integrated ocean heat content between selected layers of the entire GOM from 1950 to 2020 between 0 and 2000 m. The anomalies are related to a 1955–2006 (*WOA09*) baseline. The black line shows the linear regression fitted line based on the OHC in the upper 2000 m between 1970 and 2020. While the green line shows the fitted line between 1992 and 2017 to have the same period as ECCO data.

Linear regression is applied to the upper-2000-m OHC between 1970 and 2020 (black line, Fig. 6) and between 1992 and 2017 (green line, Fig. 6), respectively, to estimate the ocean heat storage rates in the GOM. The period of 1992 and 2017 is selected to have a common period with ECCO data for the later heat budget closure discussion. The fit between 1970 and 2020 gives us an overall heat storage rate in the past 50 years. The GOM OHC increases at 0.38 ± 0.13 ZJ decade^{-1} (mean $\pm$ uncertainty with 95% confidence interval) between 1970 and 2020 ($r = 0.76$), which is equivalent to 1.21 ± 0.41 TW (1 TW $= 10^{12}$ W). Ochoa et al. (2021) estimated the heat storage rate below 2000 m is approximately 0.17 TW ($\sim$0.054 ZJ decade^{-1}) in the GOM (uncertainty is not given in Ochoa et al. 2021). Therefore, the total heat storage rate should be approximately 1.38 ± 0.41 TW for the entire water column of the GOM between 1970 and 2020. This is equivalent to 0.86 ± 0.26 W m^{-2} if this is applied to the entire surface area of GOM (1.60×10^{12} m^2). Correspondingly, the heat storage rate between 1992 and 2017 in the GOM is approximately 0.50 ± 0.43 ZJ decade^{-1} (Fig. 6, green line), which is equivalent to 1.59 ± 1.36 TW. The full depth heat storage rate between 1992 and 2017 is about 1.76 ± 1.36 TW considering the warming below 2000 m from Ochoa et al. (2021) in the GOM or about 1.10 ± 0.85 W m^{-2} applied to the entire surface area of GOM. The ocean heat storage rate between 1992 and 2017 is larger than that for 1970–2020, primarily due to the cooling period between 1992 and 2000.

The heat storage rates between 1970 and 2020 and between 1992 and 2017 (common period of ECCO) in the GOM are both comparable to the full-depth ocean heat storage rate for the global ocean estimated from observations between 1993 and 2020 by seven different research groups, which is 0.82 to 1.11 W m^{-2} (Johnson et al. 2021) applied to the global ocean surface (3.61×10^{14} m^2). See Table 3.2 in Johnson et al. (2021) for more details about the trends of OHC increase for the global ocean. Note in Johnson et al. (2021), the ocean heat storage rate is applied to Earth's entire surface. To compare ocean to ocean rate, we converted the values in Johnson et al. (2021) to values for the global ocean surface. Although SST (Fig. 3) in the GOM suggest that the surface GOM is warming at a rate approximately twice that of the global ocean, the full-depth ocean heat storage rate in the Gulf of Mexico is similar to the rate for the global ocean.

2) NET ADVECTIVE HEAT FLUX

Based on Eq. (5), an accurate estimate of net advective heat flux requires long-term simultaneous measurements of ocean current and temperature profiles at both the Yucatán Channel and the Straits of Florida. Such observations are rare. The observations that have been conducted are mostly short term (several months to several years) and focus on current observations across the Yucatán Channel to quantify the Loop Current transport through the GOM. One of the early efforts to measure the transport through the Yucatán Channel was conducted between 1999 and 2001 with an average transport estimated to be 23.8 Sv (1 Sv $\equiv 10^6$ m^3 s^{-1}) (Sheinbaum et al. 2002). Two latter efforts with more instruments were conducted between May 2010 and May 2011 and between July 2012 and June 2013 with estimated transport to be 27.1 and 25.0 Sv, respectively (Athié et al. 2015). The variability in transport at Yucatán Channel was found to be well correlated with a transport proxy based on altimetry data (Athié et al. 2015). The most recent observations were carried out between September 2012 and August 2016 by Candela et al. (2019) across both Yucatán Channel and Straits of Florida. The average transport at both channels was 27.6 Sv based on the four years of continuous observations. The transports though the western ends of Straits of Florida were estimated to be $\sim$25 Sv for an 11-month period between December 1990 and November 1991 (Hamilton et al. 2005), which also agreed well with transport across Yucatán Channel. A long-term monitoring program measured daily flow between Florida and the Bahamas at the Cable section ($\sim$26.7°N), which can be considered as a surrogate for the Loop Current flow. The Cable estimated annual mean flow is approximately 31–32 Sv (Schmitz and McCartney 1993; Larsen and Sanford 1985; Volkov et al. 2020), which should be slightly larger than the actual Loop Current flow at the Yucatán Channel or Straits of Florida due to the inputs from the Old Bahama and the Northwest Providence Channels (Hamilton et al. 2005; Candela et al. 2019). From these limited observations, the transport flow through the GOM via the two channels may range from 23.8 to less than 32 Sv. We will use $V = 27.6 \pm 4.0$ Sv as the Loop Current transport flow in our following calculation by considering the value in Candela et al. (2019) is based on the longest (4 years) observations at both Yucatán Channel and Florida Straits and also considering the large variations from other studies. We assume the transport through Yucatán Channel and Straits of Florida are the same (Bunge et al. 2002).

To calculate the advective heat flux Qv, we also need to know the average climatology temperature difference between

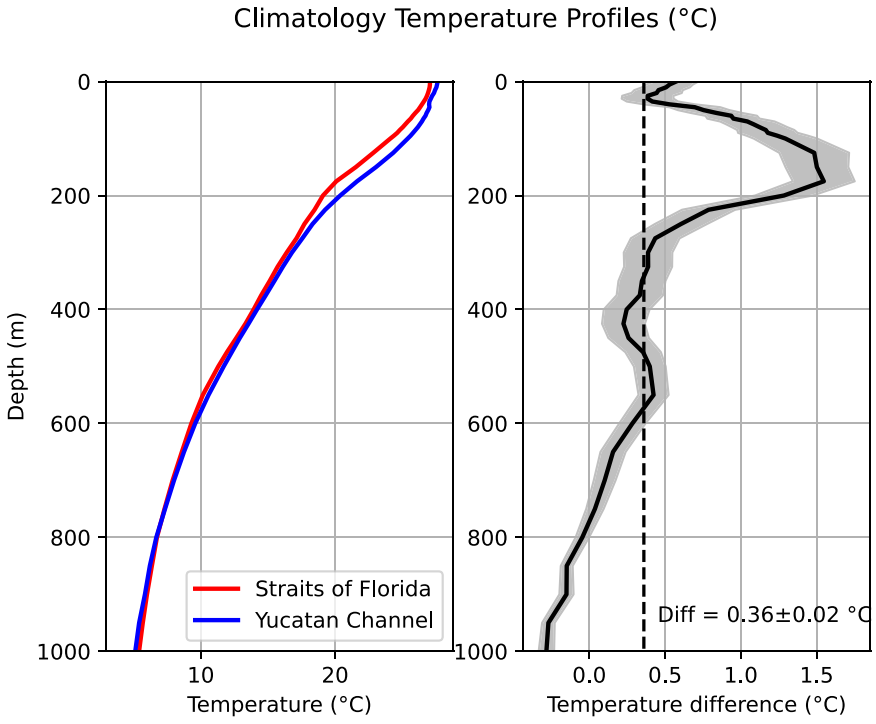

FIG. 7. (a) Climatological mean temperature profiles at Straits of Florida and Yucatán Channel in the upper 1000 m. (b) The temperature difference between the Yucatán Channel and the Straits of Florida. The shaded area shows ±1 standard deviation (std). The dashed vertical is the vertical mean of the temperature difference. 0.1° × °0.1° regional climatological temperature fields for the GOM (https://www.ncei.noaa.gov/products/gulf-mexico-regional-climatology) are used. The profile for Straits of Florida is averaged from all profiles within an area with latitudes between 23° and 25°N and longitudes between 81.1° and 80.2°W. The profile for Yucatán Channel is averaged from all profiles within an area with latitudes of 21°–21.9°N and longitudes of 86.8°–84.9°W.

the Yucatán Channel and the Straits of Florida (Fig. 7). We use the 0.1° × 0.1° GOM Regional Climatology V2 temperature fields in our analysis, which is also derived from the WOD18 using the same temperature profiles used in the above warming trend estimation. The average vertical temperature profiles at the two channels are similar with the maximum difference found between 50 and 300 m (Fig. 7). The vertical mean temperature difference δT in the upper 1000 m is approximately 0.36° ± 0.02°C (Fig. 7b). The temperature difference is calculated only in the upper 1000 m because the sill depth at the Florida Straits is only about 1000 m (730 m at its shallowest point). There might be small compensation deep flows into the Caribbean Sea below 1000 m at the Yucatán Channel (Maul et al. 1985; Bunge et al. 2002). Candela et al. (2019) showed that deep circulation contributes minimally to the overall transport of the Loop Current and therefore is not considered in this simplified calculation. Abascal et al. (2003) showed the water temperature at a given depth was cooler at the Yucatan coast and the transport was more concentrated near the Yucatan coast. We did not consider variations in the advective heat flux calculation due to the across-strait structure of the temperature section at two channels when calculating the mean temperature profile difference, which might introduce some errors/uncertainties. Substituting $V = 27.6 \pm 4.0$ Sv and $\delta T = 0.36° \pm 0.02$°C into Eq. (5), we estimate the advective net heat flux Qv to be 40.7 ± 6.3 TW. Climate models estimated Loop Current advective heat flux through the GOM in the late twentieth century to be 54.9 TW using high-resolution model or 24.9 TW if low-resolution model is used (Liu et al. 2012). Our estimate lies between the two model estimates.

Liu et al. (2012) discussed that the advection flow (Loop Current) into the GOM may slow down (20%–25% reduction) in the late twenty-first century based on climate model predictions. The consequence of a weakening Loop Current is less advective heat flux into the GOM and a cooling impact in the GOM, particularly in the northern basin based on the high-resolution Miami Isopycnic Coordinate Ocean Model (Liu et al. 2012). The transport flow observations at the Yucatán Channel (Sheinbaum et al. 2002; Athié et al. 2015; Candela et al. 2019) and the Florida Cable observations (Larsen and Sanford 1985; Volkov et al. 2020) did not show obvious evidence of the slowing down of the advective heat flux into the GOM. However, the northeastern GOM is indeed less affected by the warming between 1970 and 2020 (Fig. 5), which is coincidentally consistent with the prediction in Liu et al. (2012). The advective net heat flux may be affected by eddies

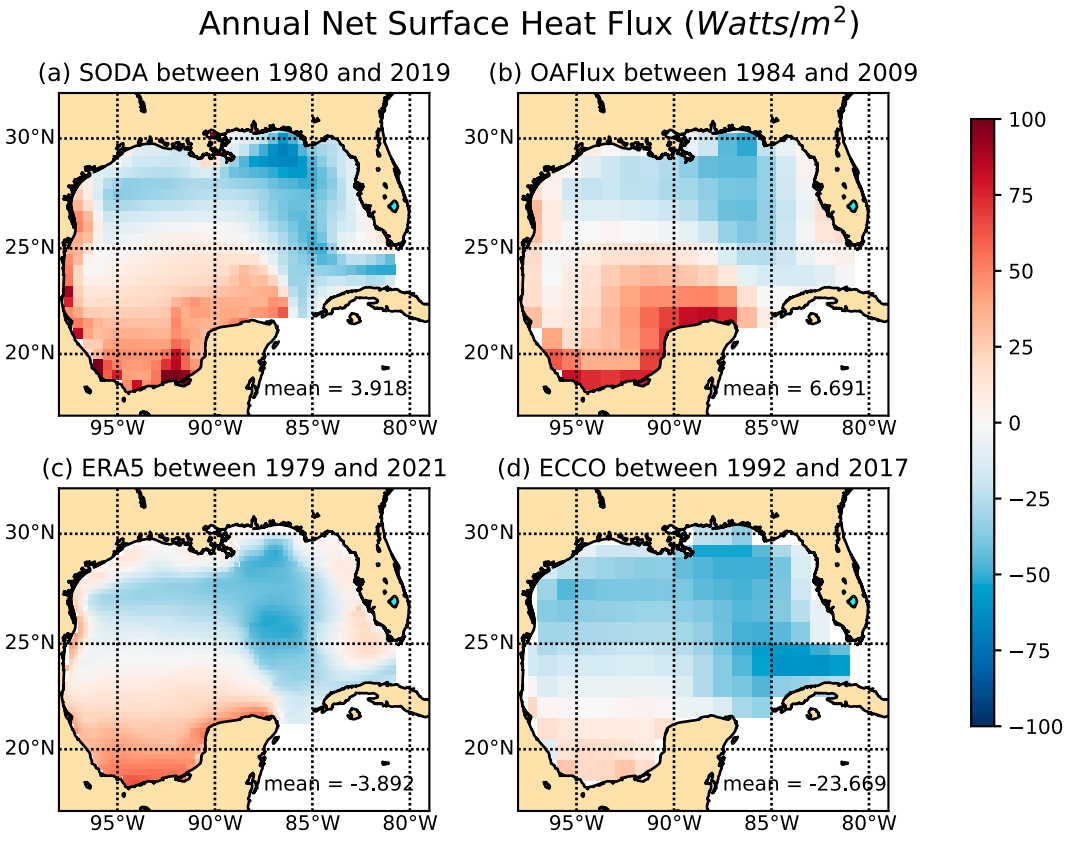

FIG. 8. Spatial distribution of the annual net surface heat flux (units: W m^{-2}) from (a) SODA, (b) OAFlux, (c) ERA5, and (d) ECCO. Note the average period is based on the available years of each dataset and shown above each panel.

and wind in the GOM and cause interannual variabilities. Using a numerical model, Chang and Oey (2010) found that a steady, uniform westward wind in the GOM could increase the heat input into the GOM via the Yucatán Channel as the wind-induced shelf currents advect more heat westward to the western Gulf. They also found eddies were effective transporters of heat across the central Gulf. Seasonality, interannual variability, and intraseasonal variability of wind fields and frequency of Loop Current eddy shedding (Zavala-Hidalgo et al. 2014) could all cause variations in the advective heat flux through the GOM, which contribute to variations of OHC in the upper ocean shown in Figs. 4 and 6.

3) NET SURFACE HEAT FLUX

We compare net surface heat flux in the GOM from four different products as listed in section 2d. All products show that the northern and eastern GOM lose heat to the atmosphere, while the southwestern GOM gains heat from the atmosphere on an annual basis (Fig. 8). It should be noted that the ECCO data show a larger heat loss area (Fig. 8d) than the other three products. The net surface heat flux averaged over the entire GOM is positive for SODA and OAFlux, but negative for ERA5 and ECCO (Fig. 8 and Table 2). The annual cycles of the net surface heat fluxes in the GOM (Fig. 9) are similar in magnitude for all products. The GOM loses heat to the atmosphere in fall, winter, and early spring and gains heat in late spring and summer. Except for ECCO, their annual mean values are centered around zero. The ECCO annual values are offset toward negative values (losing heat to the atmosphere). The long-term average values of SODA and OAFlux suggest the GOM gains heat from the atmosphere at a rate of 3.9 and 6.7 W m^{-2}, respectively, while the ERA5 loses heat to the atmosphere at a rate of −3.9 W m^{-2} annually. ECCO data show that the GOM loses a large amount of heat to the atmosphere every year at a rate of −23.7 W m^{-2}. Whether GOM gains heat from the atmosphere or loses heat to the atmosphere on an annual basis is still an open question. Previous estimates of the annual average net surface heat flux in the GOM varied from −34.1 to 46.6 W m^{-2} (Table 2) or −54.6 to 74.6 TW for the entire surface area of the GOM (area = 1.60×10^{12} m^2). Large differences might be due to the different methodologies, coefficients, formulas, and datasets used in these studies (Zavala-Hidalgo et al. 2002, 2014; Liang and Yu 2016). A heat budget analysis will help us to determine the sign of the net annual surface heat flux over the entire GOM.

4) HEAT BUDGET CLOSURE

The heat storage rate in the GOM 1.76 ± 1.36 TW between 1992 and 2017 (the same period of ECCO) based on the calculation from the OHC change in the upper 2000 m and the estimate

TABLE 2. Annual net surface heat flux from previous studies and from four global products (ERA5, SODA, OAFlux, and ECCO).

Sources	Annual surface net heat flux (W m^{-2})	Annual surface net heat flux (TW) of the entire GOM using the surface area of GOM = 1.60×10^{12} m^2
Hastenrath (1968)	−15.1	−24.2
Etter (1983)	−24.0	−38.4
Adem et al. (1993)	−2.2	−3.5
Zavala-Hidalgo et al. (2002), bulk formulas	46.6	74.6
Zavala-Hidalgo et al. (2002), satellites and empirical formulas	9.0	14.4
Liu et al. (2012), climate model, high resolution	−34.1	−54.6
Liu et al. (2012), climate model, low resolution	−18.9	−24.4
ERA5 (this study)	−3.9	−6.2
SODA (this study)	3.9	6.2
OAFlux (this study)	6.7	10.7
ECCO (this study)	−23.7	−37.9
Heat budget estimate (this study)	−24.3 ± 4.1	−38.9 ± 6.5

below 2000 m in Ochoa et al. (2021), while the advective net heat flux is estimated to be 40.7 ± 6.3 TW, which is more than 20 times larger than the heat storage rate. Based on Eq. (3), the GOM needs to release heat to the atmosphere at a rate approximately of −38.9 ± 6.5 TW; otherwise, the GOM would warm at a faster rate. Etter's (1983) estimate of −38.4 TW and the value from ECCO −37.9 TW are comparable to the estimate from Eq. (3) by taking the difference between advective net heat flux and heat storage rate between 1992 and 2017 (Table 2). Due to the fact that the average annual temperature difference between the Yucatán Channel and the Straits of Florida are almost always positive and the heat storage rate is much smaller than the advective heat flux, we would expect that the annual net surface heat flux should be negative. Based on the ocean heat closure in Eq. (3), the annual net surface heat flux from ECCO is the closest one among the four products to close the heat budget in the GOM. Note that the ECCO net surface heat flux is based on a nonlinear inverse modeling framework that satisfies both ocean

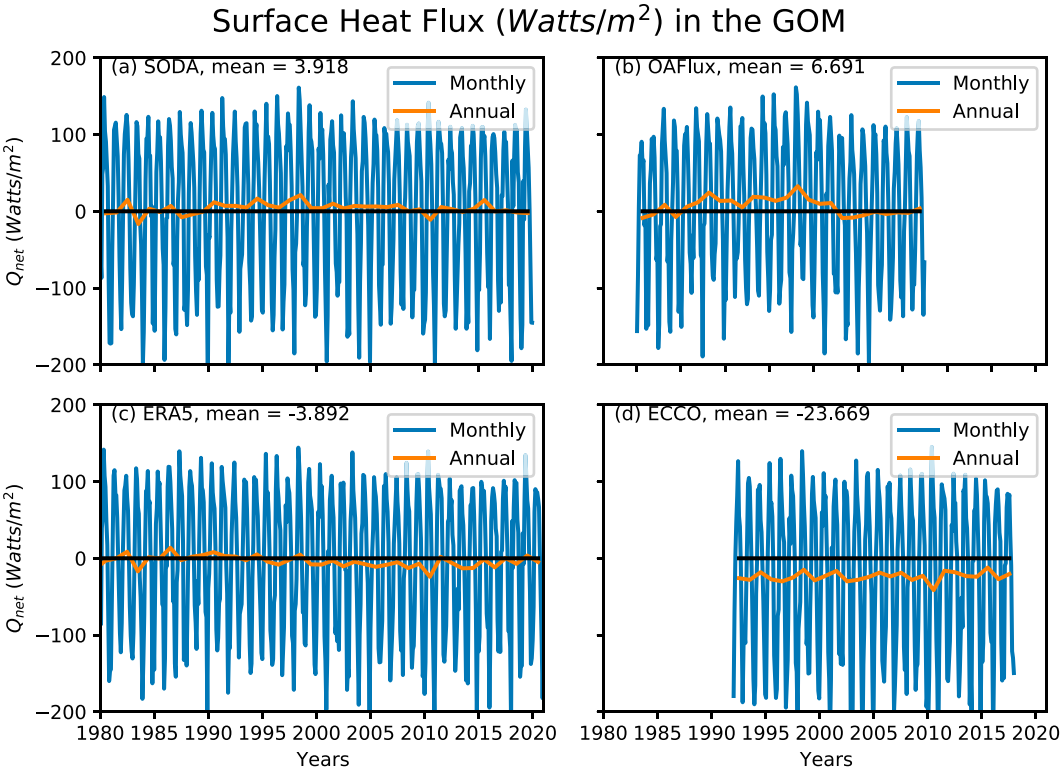

FIG. 9. Time series of monthly and annual surface heat flux for (a) SODA, (b) OAFlux, (c) ERA5, and (d) ECCO. Blue: monthly surface heat flux for the GOM; red: annual surface heat flux for the GOM. The long-term mean over the available data period for each product is shown at the top of each panel.

dynamics and data constraints (Forget et al. 2015). Wunsch (2011) also stated that the "adjoint method" used in ECCO made the resulting state estimate satisfies known equations of motion and conservation laws. That might be the reason why ECCO provides the closest net surface heat flux to close the heat budget in the GOM.

b. *Impact of warming in the GOM*

The persistent warming in the GOM (Figs. 3–6) could have already influenced the marine ecosystem and organisms in the Gulf of Mexico. Jordán-Dahlgren et al. (2005) found that surface water warming might increase the prevalence of coral diseases in the northeast Caribbean and Gulf of Mexico by enhancing pathogen activity. Warming also had negative effects on survivorship of the deep-sea coral *Lophelia pertusa* in the Gulf of Mexico based on a series of warming treatment experiments (Lunden et al. 2014). Atlantic bluefin tuna (BFT) spawns predominantly in the northern GOM with the optimal spawning temperature of 24°–27°C from April to June (Schaefer 2001). The increased upper-ocean temperature (Figs. 3 and 4) could reduce the areas in the northern GOM with BFT optimal spawning conditions (Muhling et al. 2011). Warming produces a poleward shift in the distribution of many organisms. For example, numerous additions to the fish fauna were discovered by comparing fish assemblages within seagrass meadows of the northern GOM between the 1970s and 2006/07 survey data (Fodrie et al. 2010). GOM has one of the world's largest eutrophication-driven coastal hypoxia zones and warming will only exacerbate hypoxic conditions (Boesch 2008; Laurent et al. 2018).

GOM is one of the marginal seas with frequent hurricane formations and landfalls each year. Hurricane intensity is sensitive to changes in SST (Emanuel 2005) and OHC in the upper ocean (Hallam et al. 2021; Eley et al. 2021). A 0.5°C increase in August–September SST is responsible for a 40% increase in hurricane activity and frequency (Saunders and Lea 2008) based on a statistical model. Hurricane prediction model results show the frequency of category 4 and 5 storms could be doubled by the end of the twenty-first century due to global warming, and the largest increase is projected to occur in the western Atlantic Ocean and Gulf of Mexico (Bender et al. 2010). The average SST has increased by approximately 1.0°C (Fig. 3) and the OHC increase is most prominent in the upper 200 m (Fig. 4) since the 1970s, which contribute to the recent intensified hurricane activities in the Gulf of Mexico, e.g., Hurricane Harvey (Trenberth et al. 2018) and Hurricane Michael (Nyadjro et al. 2021). Hurricane rainfall dependency increases by a factor of 5 when SSTs range from 26° to 29°C (Folkins and Braun 2003).

Although the Gulf of Mexico is a semienclosed marginal sea, its warming is sensitive to climate change in the Caribbean Sea and north tropical Atlantic Ocean (Ochoa et al. 2021; Chollett et al. 2012). Long-term monitoring of the heat transport through the Yucatán Channel is necessary to understand the controlling mechanisms of the warming in the GOM. The role of the Loop Current and Loop Current eddies in controlling the warming also needs more investigation.

5. Summary

OHC in the Gulf of Mexico is calculated from the World Ocean Database 2018 (Boyer et al. 2018) with 1° × °1° spatial resolution for the upper 2000 m and is available from 1950 to 2020. The warming/cooling trends are quantified based on the change of OHC at both basin and grid scales using a linear regression method. We have estimated a warming rate of 0.38 ± 0.13 ZJ decade^{-1} (0.76 ± 0.26 W m^{-2}) over the upper 2000 m in the GOM in 50 years between 1970 and 2020. The warming rate for the entire GOM between 1970 and 2020 is 0.86 ± 0.26 W m^{-2} (0.76 W m^{-2} in the upper 2000 m + 0.1 W m^{-2} below 2000 m; Ochoa et al. 2021), which is comparable to the warming rate of the global ocean (0.82–1.11 W m^{-2}; Johnson et al. 2021). Warming occurs at all depths from the sea surface to bottom with the largest warming rates found in the upper 50 m (Fig. 4b and Ochoa et al. 2021). The rate of the warming trend at the surface is about twice that for the global ocean (Fig. 3). A subsurface decadal warming and cooling oscillation with irregular periods is found between 200 and 600 m. Most regions of the GOM show a warming trend between 1970 and 2020, except for a subsurface region in the northeastern GOM. Based on the ocean heat budget, the GOM should lose heat to the atmosphere and the annual net negative surface heat flux from the ECCO can roughly close the heat budget in the GOM. The Loop Current advective heat flux is the main heat source for the warming in the GOM. The southern GOM gains heat from the atmosphere on the annual time scale, but integrated over the entire basin, the GOM loses heat to the atmosphere.

Understanding the spatial and temporal evolution of the warming trend in the Gulf of Mexico is critical to advance the understanding of environmental change since the 1970s. The warming in the Gulf of Mexico could cause a series of environmental issues, for example, sea level rise and the incidence of hypoxia. Warming also increases the intensity of hurricanes, which leads to the potential loss of wetlands and damage to coastal communities. Warming could cause increased stratification and reduce the O_2 solubility of the water. Less nutrients can be mixed into the surface waters due to enhanced stratification, which will have a negative impact on phytoplankton production and eventually on marine species and commercial fisheries. Here we have shown that most regions of the GOM have become warmer since the 1970s. We hope this study may inspire more investigations on the relationship between warming and environmental issues in the GOM.

Acknowledgments. This work was supported by the NOAA National Centers for Environmental Information (NCEI) and NOAA Grant 363541-191001-021000 (Northern Gulf Institute) at Mississippi State University. The authors thank the scientists and data providers for continuing to share their data, data managers and our NCEI colleagues for stewarding the data for long-term preservation, and the NCEI Ocean Climate Laboratory colleagues for continuing to enhance and maintain the World Ocean Database. Without this combined effort, data-based studies like this would not be possible. We thank S. Cross, D. Dukhovskoy, H.M. Zhang, J. Carton, and other NCEI colleagues for valuable conversations.

Data availability statement. We used the most recent version of the World Ocean Database published online in 2018 (WOD18) and available at https://www.ncei.noaa.gov/products/world-ocean-database. GOM Regional Climatology data are available at https://www.ncei.noaa.gov/products/gulf-mexico-regional-climatology. ERA5 surface heat flux is available at https://www.ecmwf.int/en/forecasts/datasets/reanalysis-datasets/era5; OAFlux is available at https://oaflux.whoi.edu/data-access/; ECCO surface heat flux is available at https://cmr.earthdata.nasa.gov/virtual-directory/collections/C1990404812-POCLOUD/temporal; and SODA data are available at https://www2.atmos.umd.edu/~ocean/index_files/soda3.4.2_mn_download_b.htm.

REFERENCES

Abascal, A. J., J. Sheinbaum, J. Candela, J. Ochoa, and A. Badan, 2003: Analysis of flow variability in the Yucatan Channel. *J. Geophys. Res.*, **108**, 3381, https://doi.org/10.1029/2003JC001922.

Adem, J., E. E. Villanueva, and V. M. Mendoza, 1993: A new method for estimating the seasonal cycle of the heat balance at the ocean surface, with application to the Gulf of Mexico. *Geofis. Int.*, **32**, 21–34, https://doi.org/10.22201/igeof.00167169p.1993.32.1.1149.

Alory, G., and G. Meyers, 2009: Warming of the upper equatorial Indian Ocean and changes in the heat budget (1960–99). *J. Climate*, **22**, 93–113, https://doi.org/10.1175/2008JCLI2330.1.

Athié, G., J. Sheinbaum, R. Leben, J. Ochoa, M. R. Shannon, and J. Candela, 2015: Interannual variability in the Yucatan Channel flow. *Geophys. Res. Lett.*, **42**, 1496–1503, https://doi.org/10.1002/2014GL062674.

Bender, M. A., T. R. Knutson, R. E. Tuleya, J. J. Sirutis, G. A. Vecchi, S. T. Garner, and I. M. Held, 2010: Modeled impact of anthropogenic warming on the frequency of intense Atlantic hurricanes. *Science*, **327**, 454–458, https://doi.org/10.1126/science.1180568.

Boesch, D. F., 2008: Global warming and coastal dead zones. *National Wetlands Newsletter*, Vol. 30, No. 4, Environmental Law Institute, Washington, DC, 11–13, 21, http://www.umces.edu/sites/default/files/pdfs/db_WarmingDeadZones.pdf.

Boyer, T. P., and Coauthors, 2018: World Ocean Database 2018. NOAA Atlas NESDIS 87, 207 pp.

Bunge, L., J. Ochoa, A. Badan, J. Candela, and J. Sheinbaum, 2002: Deep flows in the Yucatan Channel and their relation to changes in the Loop Current extension. *J. Geophys. Res.*, **107**, 3233, https://doi.org/10.1029/2001JC001256.

Candela, J., and Coauthors, 2019: The flow through the Gulf of Mexico. *J. Phys. Oceanogr.*, **49**, 1381–1401, https://doi.org/10.1175/JPO-D-18-0189.1.

Carton, J. A., G. A. Chepurin, L. Chen, and S. A. Grodsky, 2018: Improved global net surface heat flux. *J. Geophys. Res. Oceans*, **123**, 3144–3163, https://doi.org/10.1002/2017JC013137.

Chang, Y. L., and L. Y. Oey, 2010: Eddy and wind-forced heat transports in the Gulf of Mexico. *J. Phys. Oceanogr.*, **40**, 2728–2742, https://doi.org/10.1175/2010JPO4474.1.

Chollett, I., F. E. Müller-Karger, S. F. Heron, W. Skirving, and P. J. Mumby, 2012: Seasonal and spatial heterogeneity of recent sea surface temperature trends in the Caribbean Sea and southeast Gulf of Mexico. *Mar. Pollut. Bull.*, **64**, 956–965, https://doi.org/10.1016/j.marpolbul.2012.02.016.

Cohen, D., 2018: Coastline county population continues to grow. U.S. Census Bureau, accessed 30 November 2019, https://www.census.gov/library/stories/2018/08/coastal-county-populationrises.html.

Eley, E. N., B. Subrahmanyam, and C. B. Trott, 2021: Ocean–atmosphere interactions during Hurricanes Marco and Laura (2020). *Remote Sens.*, **13**, 1932, https://doi.org/10.3390/rs13101932.

Emanuel, K., 2005: *Divine Wind: The History and Science of Hurricanes*. Oxford University Press, 296 pp.

Etter, P. C., 1983: Heat and freshwater budgets of the Gulf of Mexico. *J. Phys. Oceanogr.*, **13**, 2058–2069, https://doi.org/10.1175/1520-0485(1983)013<2058:HAFBOT>2.0.CO;2.

Fodrie, F. J., K. L. Heck Jr., S. P. Powers, W. M. Graham, and K. L. Robinson, 2010: Climate-related, decadal-scale assemblage changes of seagrass-associated fishes in the northern Gulf of Mexico. *Global Change Biol.*, **16**, 48–59, https://doi.org/10.1111/j.1365-2486.2009.01889.x.

Folkins, I., and C. Braun, 2003: Tropical rainfall and boundary layer moist entropy. *J. Climate*, **16**, 1807–1820, https://doi.org/10.1175/1520-0442(2003)016<1807:TRABLM>2.0.CO;2.

Forget, G. A. E. L., J. M. Campin, P. Heimbach, C. N. Hill, R. M. Ponte, and C. Wunsch, 2015: ECCO version 4: An integrated framework for non-linear inverse modeling and global ocean state estimation. *Geosci. Model Dev.*, **8**, 3071–3104, https://doi.org/10.5194/gmd-8-3071-2015.

Glenn, E., D. Comarazamy, J. E. González, and T. Smith, 2015: Detection of recent regional sea surface temperature warming in the Caribbean and surrounding region. *Geophys. Res. Lett.*, **42**, 6785–6792, https://doi.org/10.1002/2015GL065002.

Hallam, S., M. Guishard, S. A. Josey, P. Hyder, and J. Hirschi, 2021: Increasing tropical cyclone intensity and potential intensity in the subtropical Atlantic around Bermuda from an ocean heat content perspective 1955–2019. *Environ. Res. Lett.*, **16**, 034052, https://doi.org/10.1088/1748-9326/abe493.

Hamilton, P., J. C. Larsen, K. D. Leaman, T. N. Lee, and E. Waddell, 2005: Transports through the Straits of Florida. *J. Phys. Oceanogr.*, **35**, 308–322, https://doi.org/10.1175/JPO-2688.1.

Hastenrath, S. L., 1968: Estimates of the latent and sensible heat flux for the Caribbean Sea and the Gulf of Mexico. *Limnol. Oceanogr.*, **13**, 322–331, https://doi.org/10.4319/lo.1968.13.2.0322.

Hersbach, H., and Coauthors, 2020: The ERA5 global reanalysis. *Quart. J. Roy. Meteor. Soc.*, **146**, 1999–2049, https://doi.org/10.1002/qj.3803.

Hurrell, J. W., 1995: Decadal trends in the North Atlantic Oscillation: Regional temperatures and precipitation. *Science*, **269**, 676–679, https://doi.org/10.1126/science.269.5224.676.

IPCC, 2021: *Climate Change 2021: The Physical Science Basis*. V. Masson-Delmotte et al., Eds., Cambridge University Press, 3949 pp.

Johnson, G. C., J. M. Lyman, T. Boyer, L. Cheng, J. Gilson, M. Ishii, R. E. Killick, and S. G. Purkey, 2021: Ocean heat content [in "State of the Climate in 2020"]. *Bull. Amer. Meteor. Soc.*, **102** (8), S156–S159, https://doi.org/10.1175/2021BAMSStateoftheClimate.1.

Jordán-Dahlgren, E., M. A. Maldonado, and R. E. Rodríguez-Martínez, 2005: Diseases and partial mortality in *Montastraea annularis* species complex in reefs with differing environmental conditions (NW Caribbean and Gulf of México). *Dis. Aquat. Org.*, **63**, 3–12, https://doi.org/10.3354/dao063003.

Kuffner, I. B., B. H. Lidz, J. H. Hudson, and J. S. Anderson, 2015: A century of ocean warming on Florida Keys coral reefs: Historic in situ observations. *Estuaries Coasts*, **38**, 1085–1096, https://doi.org/10.1007/s12237-014-9875-5.

Larsen, J. C., and T. B. Sanford, 1985: Florida Current volume transports from voltage measurements. *Science*, **227**, 302–304, https://doi.org/10.1126/science.227.4684.302.

Laurent, A., K. Fennel, D. S. Ko, and J. Lehrter, 2018: Climate change projected to exacerbate impacts of coastal eutrophication in the northern Gulf of Mexico. *J. Geophys. Res. Oceans*, **123**, 3408–3426, https://doi.org/10.1002/2017JC013583.

Lee, C. M., and D. L. Rudnick, 2018: Underwater gliders. *Observing the Oceans in Real Time*, R. Venkatesan et al., Eds., Springer Oceanography, Springer, 129–139, https://doi.org/10.1007/978-3-319-66493-4_7.

Levitus, S., J. I. Antonov, T. P. Boyer, R. A. Locarnini, H. E. Garcia, and A. V. Mishonov, 2009: Global ocean heat content 1955–2008 in light of recently revealed instrumentation problems. *Geophys. Res. Lett.*, **36**, L07608, https://doi.org/10.1029/2008GL037155.

——, and Coauthors, 2012: World Ocean heat content and thermosteric sea level change (0–2000 m), 1955–2010. *Geophys. Res. Lett.*, **39**, L10603, https://doi.org/10.1029/2012GL051106.

Li, G., Z. Wang, and B. Wang, 2022: Multidecade trends of sea surface temperature, chlorophyll-a concentration, and ocean eddies in the Gulf of Mexico. *Remote Sens.*, **14**, 3754, https://doi.org/10.3390/rs14153754.

Liang, X., and L. Yu, 2016: Variations of the global net air–sea heat flux during the "hiatus" period (2001–10). *J. Climate*, **29**, 3647–3660, https://doi.org/10.1175/JCLI-D-15-0626.1.

Liu, Y., S. K. Lee, B. A. Muhling, J. T. Lamkin, and D. B. Enfield, 2012: Significant reduction of the Loop Current in the 21st century and its impact on the Gulf of Mexico. *J. Geophys. Res.*, **117**, C05039, https://doi.org/10.1029/2011JC007555.

Locarnini, R. A., and Coauthors, 2018: *Temperature*. Vol. 1, *World Ocean Atlas 2018*, NOAA Atlas NESDIS 81, 52 pp.

Lunden, J. J., C. G. McNicholl, C. R. Sears, C. L. Morrison, and E. E. Cordes, 2014: Acute survivorship of the deep-sea coral *Lophelia pertusa* from the Gulf of Mexico under acidification, warming, and deoxygenation. *Front. Mar. Sci.*, **1**, 78, https://doi.org/10.3389/fmars.2014.00078.

Maul, G. A., D. A. Mayer, and S. R. Baig, 1985: Comparisons between a continuous 3-year current-meter observation at the sill of the Yucatan Strait, satellite measurements of Gulf Loop Current area, and regional sea level. *J. Geophys. Res.*, **90**, 9089–9096, https://doi.org/10.1029/JC090iC05p09089.

McCarthy, G. D., I. D. Haigh, J. J. M. Hirschi, J. P. Grist, and D. A. Smeed, 2015: Ocean impact on decadal Atlantic climate variability revealed by sea-level observations. *Nature*, **521**, 508–510, https://doi.org/10.1038/nature14491.

McKinney, L. D., and Coauthors, 2021: The Gulf of Mexico. *Oceanography*, **34** (1), 30–43, https://doi.org/10.5670/oceanog.2021.115.

Muhling, B. A., S. K. Lee, J. T. Lamkin, and Y. Liu, 2011: Predicting the effects of climate change on bluefin tuna (*Thunnus thynnus*) spawning habitat in the Gulf of Mexico. *ICES J. Mar. Sci.*, **68**, 1051–1062, https://doi.org/10.1093/icesjms/fsr008.

Muller-Karger, F. E., and Coauthors, 2015: Natural variability of surface oceanographic conditions in the offshore Gulf of Mexico. *Prog. Oceanogr.*, **134**, 54–76, https://doi.org/10.1016/j.pocean.2014.12.007.

Nyadjro, E. S., Z. Wang, J. Reagan, J. Cebrian, and J. F. Shriver, 2021: Bio-physical changes in the Gulf of Mexico during the 2018 Hurricane Michael. *IEEE Geosci. Remote Sens. Lett.*, **19**, 1–5, https://doi.org/10.1109/LGRS.2021.3068600.

Ochoa, J., V. Ferreira-Bartrina, J. Candela, J. Sheinbaum, M. López, P. Pérez-Brunius, S. Herzka, and R. M. W. Amon, 2021: Deep-water warming in the Gulf of Mexico from 2003 to 2019. *J. Phys. Oceanogr.*, **51**, 1021–1035, https://doi.org/10.1175/JPO-D-19-0295.1.

Panofsky, H. A., and G. W. Brier, 1958: *Some Applications of Statistics to Meteorology*. Pennsylvania State University, 224 pp.

Poore, R. Z., and J. C. Brock, 2011: Evidence of multidecadal climate variability in the Gulf of Mexico. U.S. Geological Survey Fact Sheet 2011-3027, 2 pp., https://pubs.usgs.gov/fs/2011/3027/.

Saunders, M. A., and A. S. Lea, 2008: Large contribution of sea surface warming to recent increase in Atlantic hurricane activity. *Nature*, **451**, 557–560, https://doi.org/10.1038/nature06422.

Schaefer, K. M., 2001: Reproductive biology of tunas. *Fish Physiol.*, **19**, 225–270, https://doi.org/10.1016/S1546-5098(01)19007-2.

Schmitz, W. J., Jr., and M. S. McCartney, 1993: On the North Atlantic circulation. *Rev. Geophys.*, **31**, 29–49, https://doi.org/10.1029/92RG02583.

Seidov, D., A. Mishonov, and R. Parsons, 2021: Recent warming and decadal variability of Gulf of Maine and slope water. *Limnol. Oceanogr.*, **66**, 3472–3488, https://doi.org/10.1002/lno.11892.

Sheinbaum, J., J. Candela, A. Badan, and J. Ochoa, 2002: Flow structure and transport in the Yucatan Channel. *Geophys. Res. Lett.*, **29**, 1040, https://doi.org/10.1029/2001GL013990.

Trenberth, K. E., L. Cheng, P. Jacobs, Y. Zhang, and J. Fasullo, 2018: Hurricane Harvey links to ocean heat content and climate change adaptation. *Earth's Future*, **6**, 730–744, https://doi.org/10.1029/2018EF000825.

Volkov, D. L., R. Domingues, C. S. Meinen, R. Garcia, M. Baringer, G. Goni, and R. H. Smith, 2020: Inferring Florida Current volume transport from satellite altimetry. *J. Geophys. Res. Oceans*, **125**, e2020JC016763, https://doi.org/10.1029/2020JC016763.

Wong, A. P., and Coauthors, 2020: Argo data 1999–2019: Two million temperature-salinity profiles and subsurface velocity observations from a global array of profiling floats. *Front. Mar. Sci.*, **7**, 700, https://doi.org/10.3389/fmars.2020.00700.

Wunsch, C., 2011: The decadal mean ocean circulation and Sverdrup balance. *J. Mar. Res.*, **69**, 417–434, https://doi.org/10.1357/002224011798765303.

Yu, L., X. Jin, and R. A. Weller, 2008: Multidecade global flux datasets from the objectively analyzed air-sea fluxes (OAFlux) project: Latent and sensible heat fluxes, ocean evaporation, and related surface meteorological variables. Woods Hole Oceanographic Institution OAFlux Project Tech. Rep. OA-2008-1, 64 pp.

Zavala-Hidalgo, J., A. Pares-Sierra, and J. Ochoa, 2002: Seasonal variability of the temperature and heat fluxes in the Gulf of Mexico. *Atmósfera*, **15**, 81–104.

——, R. Romero-Centeno, A. Mateos-Jasso, S. L. Morey, and B. Martínez-López, 2014: The response of the Gulf of Mexico to wind and heat flux forcing: What has been learned in recent years? *Atmósfera*, **27**, 317–334, https://doi.org/10.1016/S0187-6236(14)71119-1.